metals

MDPI

Article

The Microstructural Refinement of the A356 Alloy Using Semi-Solid and Severe Plastic-Deformation Processing

Mohamed Abdelgawad Gebril [1,*], Mohd Zaidi Omar [2], Intan Fadhlina Mohamed [2], Norinsan Kamil Othman [3], Ahmad Muhammad Aziz [2] and Osama M. Irfan [4,5,*]

[1] Department of Mechanical Engineering, Faculty of Engineering, University of Benghazi, Benghazi 16063, Libya
[2] Department of Mechanical and Manufacturing Engineering, Faculty of Engineering and Built Environment, Universiti Kebangsaan Malaysia, Bangi 43600, Selangor, Malaysia; zaidiomar@ukm.edu.my (M.Z.O.); intanfadhlina@ukm.edu.my or intan@ukm.edu.my (I.F.M.); ahmadmuhammadaziz@gmail.com (A.M.A.)
[3] Department of Applied Physics, Faculty of Science and Technology, Universiti Kebangsaan Malaysia, Bangi 43600, Selangor, Malaysia; insan@ukm.edu.my
[4] Department of Mechanical Engineering, College of Engineering, Qassim University, Buraydah 51452, Saudi Arabia
[5] Mechanical Department, Beni Suef University, Beni Suef 62746, Egypt
* Correspondence: mohamed.almalki@uob.edu.ly (M.A.G.); o.ahmed@qu.edu.sa (O.M.I.); Tel.: +218-9208-51348 (M.A.G.); +966-566-280-516 (O.M.I.)

Abstract: Improving the engineering properties of A356 alloy is an appealing option for the automotive industry. This study aimed at refining and redistributing Si particles and the eutectic phase by applying T6 heat treatment to a semi-solid A356 alloy, followed by severe plastic deformation (SPD). Using a cooling-slope technique, the as-cast and rheocast samples were subjected to heat treatment prior to being processed using equal-channel angular pressing (ECAP) and high-pressure torsion (HPT) at room temperature. The results show that the brittle Si particles were effectively fragmented and redistributed in the homogenous microstructure. The grain size reduced from 170 µm to 23 µm in the as-cast sample after combining heat treatment and the cooling-slope. This was followed by the ECAP sample after six passes through route A (where the sample is not rotated between each pass), while it reduced to 160 nm after five turns of the HPT process in a heat-treated cooling-slope sample. The hardness of the heat-treated cooling-slope casting samples increased with the ECAP process; there was an increase from 61 HV to 134 HV for the as-cast alloy after six passes through route A. The hardness of the heat-treated cooling-slope sample improved with the HPT process to 211 HV after five turns.

Keywords: A356 alloy; semi-solid; heat treatment; ECAP; HPT; hardness

check for updates

Citation: Gebril, M.A.; Omar, M.Z.; Mohamed, I.F.; Othman, N.K.; Aziz, A.M.; Irfan, O.M. The Microstructural Refinement of the A356 Alloy Using Semi-Solid and Severe Plastic-Deformation Processing. *Metals* **2023**, *13*, 1843. https://doi.org/10.3390/met13111843

Academic Editors: Marcello Cabibbo, Ayrat Nazarov and Wenchao Yang

Received: 31 August 2023
Revised: 20 October 2023
Accepted: 25 October 2023
Published: 2 November 2023

Copyright: © 2023 by the authors. Licensee MDPI, Basel, Switzerland. This article is an open access article distributed under the terms and conditions of the Creative Commons Attribution (CC BY) license (https://creativecommons.org/licenses/by/4.0/).

1. Introduction

The A356 alloy is used extensively in the manufacture of automotive components, for instance, chassis and engine parts, where the components are produced using different casting processes. It is worth noting that the presence of primary dendritic-shaped α-Al, which is encircled by a eutectic second-phase Si in a flaky morphology, reduces the fracture toughness and strength of hypoeutectic Al–Si alloys. Premature cracking can occur due to the presence of rough and flaky Si particles when the material is subjected to deformation. This can lead to the decreased processability of the alloy at ambient temperatures, ultimately affecting its ductility [1,2]. The crucial factors affecting the corrosion resistance and electrochemical properties of the Al–Si alloy are the distribution and shape of Si particles. Improving the engineering properties of the Al–Si alloy by refining its microstructure is a challenge in the industry. The most commonly used technique for this is the semi-solid process, wherein the primary α-Al grains transform from a dendritic to a spherical shape.

Additionally, the eutectic Si particles become more acicular-like in shape [3]. Multiple techniques for achieving an appropriate (not dendritic) microstructure have been developed. One of these technologies is the cooling-slope casting (CS) process, a simple semi-solid metal casting process; this process requires minimal equipment and has a low operational cost [3–6]. Processing semi-solid materials has the potential to significantly improve their mechanical properties [6–9]. Al–Si alloys can be treated with heat to improve their properties. Heat treatment can be applied to modify the morphology of eutectic Si particles and certain intermetallic compounds since this could result in the improved strength of aluminium alloys through ageing processes [10]. The spheroids of the Si particles during the T6 heat treatment in Al–Si cast alloys are the main reason for the good fracture elongation [11,12]. Deformation processing has proven to be highly effective in enhancing the mechanical properties of hypoeutectic Al–Si alloys by refining and homogenising their microstructure [13,14], through ultrafine grains and the distribution of the refined eutectic phase. In the field of severe plastic deformation (SPD), two common processes used are equal-channel angular pressing (ECAP) and high-pressure torsion (HPT). By refining the microstructure and evenly dispersing the eutectic phase, the mechanical properties of the A356 alloy are enhanced through the (SPD) process [12,15–17]. A few limited studies have applied the combination of semi-solid and ECAP processes to improve the mechanical properties [17,18]. Subjecting the A356 alloy to heat treatment (annealing) together with ECAP results in the improved hardness and wear-resistance of the alloy [19]. The aim of this study was to achieve the following objectives: First, investigate the microstructural refinement of the A356 alloy using a semi-solid process before and after T6 heat treatment. Second, evaluate the microstructural refinement of as-cast and semi-solid A356 alloys before and after T6 heat treatment, followed by ECAP and HPT processing. Third, study the effect of semi-solid and heat treatment combined, followed by (SPD), on the microhardness distribution of an Al 356 alloy.

2. Materials and Methods

This study employed a cast commercial A356 (Si-6.7 wt. %, Mg-0.23 wt. %, Ti-0.178 wt. %, Fe-0.126 wt. %, Cu-0.01 wt. %) alloy with an ingot shape melted at a temperature of 750 °C in a graphite crucible. The moulted alloy was then poured at 620 °C at an angle of 60° on a 250 mm-length cooling-slope plate made of stainless steel. The selection of these conditions is based on our research and findings [9,20]. A mould for the molten alloy was positioned at the bottom of the cooling-slope plate, where it was quenched immediately in water at room temperature. Both the as-cast and cooling-slope samples were subjected to T6 thermal treatment in this study, involving the following procedures: (1) solution treatment at 540 °C for 8-h, (2) rapid quenching in water, and (3) ageing treatment at 180 °C for 3-h [21]. Following that, using an electrical discharge machine (EDM), the as-cast and cooling-slope samples were machined to a 10 mm diameter with a 1 mm thickness for microstructure analysis and hardness testing. The ECAP die consists of two intersecting channels, a plunger, and a hydraulic press. The two intersecting channels have an internal angle (Φ) = 120° and an outer angle (Ψ) = 20°. A heat-treated tool steel was used to create the die and plunger, giving it a Rockwell hardness of ~55. The as-cast and cooling-slope samples were fabricated using EDM, resulting in rods with a length of 12 cm and a diameter of 9.8 mm. The sample and plunger were completely lubricated with molybdenum disulphide (MoS_2) grease prior to pressing.

The entire ECAP process was conducted at room temperature. Each individual passage through the die in the ECAP process resulted in an applied strain of 0.62 due to the geometry and angles. The samples were processed using route A, whereby the samples were not rotated between passes. Before undergoing the HPT process, both the as-cast and cooling-slope samples were cut using an EDM machine. The samples were cut into diameters of 10 mm, with a thickness of 1.0 mm. The following HPT process was conducted under normal conditions at room temperature. Under 6.0 GPa pressure and 1.0 rpm rotation speed, 0.75 and 5 turns of the HPT process were completed. The microstructure of the

samples was examined using three sets of microscopes: firstly, an optical microscope (OM, Olympus Corporation, Tokyo, Japan); secondly, a field emission scanning electron microscope (FESEM, Zeiss, Oberkochen, Germany); and lastly, a field emission transmission electron microscope (FETEM, JEOL, JEM-2100F, Tokyo, Japan). Sample preparation for microstructure observation included the samples being ground using silicon carbide (SiC) sandpaper with a grit range of 180 and 2000, and they were polished to produce a mirror-like surface using diamond paste of 3 μm and 1 μm for OM and FESEM analysis. Keller's reagent (1% HF, 1.5% HCl, 2.5% HNO_3, H_2O solution) was used as an etchant to carry out the etching process. However, for FETEM analysis, the samples were ground to 0.12 mm, and then thinned using a twin-jet electro-polisher in a solution of 20% NHO_3 and 80% CH_3OH. The process was performed at a freezing temperature of −13 degrees Celsius, while applying a voltage of 12 volts. The sample for the microstructure analysis was taken in the centre and on the edge of the disk. The analysis of quantitative metallography was conducted according to the ASTM E112 standard to measure the size of the grains. Using the Smart Tiffv2 software, the length and width of the Si particles were measured, taking into account at least 200 particles in each case. Then, Vickers microhardness (HV) testing was performed (micro-Vickers hardness tester, Zwick, Germany; ZHVμ), which involved applying a 100 g load for 15 s. As indicated in Figure 1, there were four radial indentations, with each one being equidistant from the centre to the edge of the disk in the four radial directions. The hardness values were obtained by averaging three samples for each case.

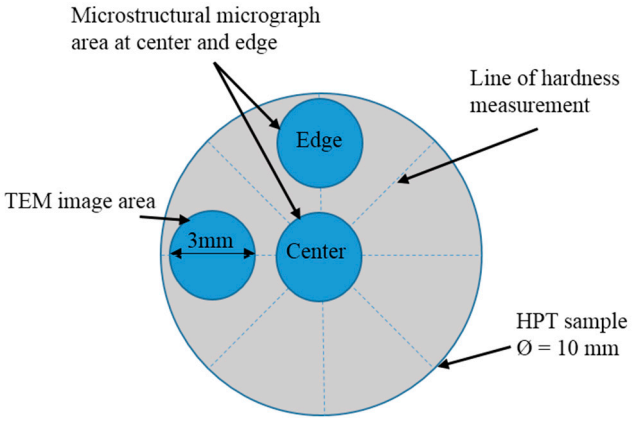


Figure 1. Schematic diagram of the HPT disk including hardness measurement locations and microstructure regions.

3. Results and Discussion

3.1. Microstructural Evaluation of the As-Cast Alloy

The optical micrograph in Figure 2 shows low and high magnifications of the as-cast A356 alloy. The microstructure of the A356 alloy exhibits the typical hypoeutectic dendritic bright phase of the α-Al phase enclosed by dark eutectic phase, including acicular and flaky Si particles and secondary intermetallic compounds. The dendritic α-Al phase was approximately 170.5 μm in size with a rough eutectic phase. The FESEM and EDS analyses of the samples were carried out to conduct a comprehensive assessment of the intermetallic phases with different shapes. The eutectic phase in the A356 alloy consisted of eutectic Si particles and several intermetallic particles that may precipitate during solidification. Mechanical properties of Al–Si alloys are strongly influenced by the intermetallic compounds present in the alloys. These compounds are produced by adding elements such as iron, magnesium, and copper to an Al–Si alloy in order to improve its strength. Figure 3 shows SEM images of the A356 alloy microstructure and the EDS spectrums corresponding with the analysis phases. The chemical compositions of the analysed phases of Figure 3 are shown in Table 1.

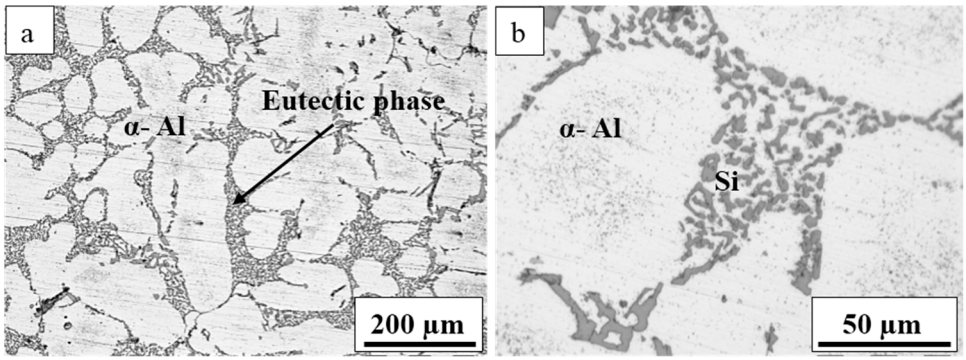


Figure 2. Optical micrograph of the as-cast A356 alloy at (**a**) low and (**b**) high magnification.

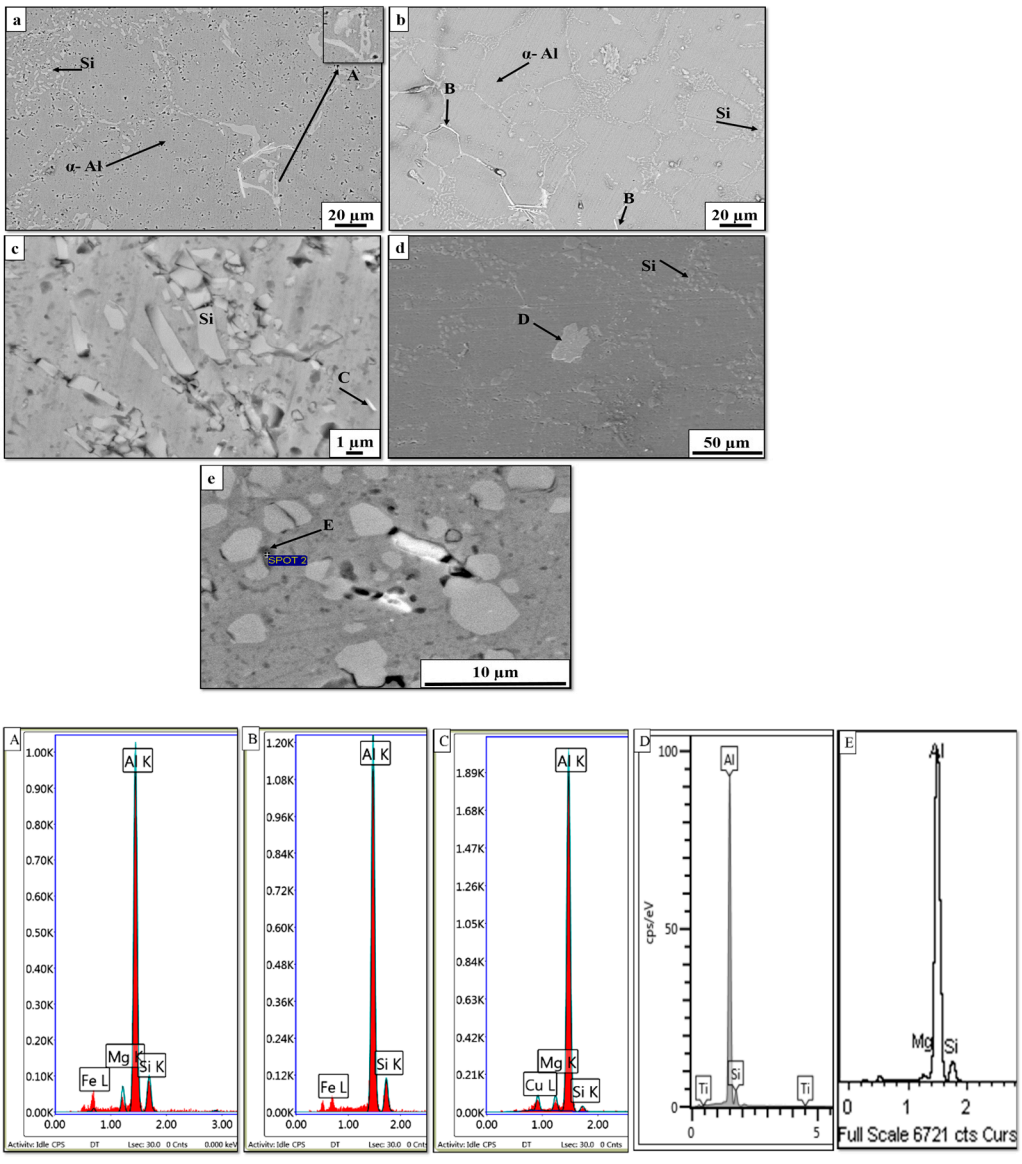


Figure 3. SEM morphology of (**a**–**e**) alloy A356 alloy and the corresponding EDS results for (**A**) π-AlFeSiMg, (**B**) β-Al_5FeSi, (**C**) Al_2Cu, (**D**) Al_3Ti, and (**E**) Mg_2Si, respectively.

Table 1. The chemical compositions (wt. %) of the analysed phases.

Spectrum	Mg	Al	Si	Fe	Cu	Ti
A	1.56	68.54	10.35	19.55	-	1.56
B	-	74.14	11.47	14.39	-	-
C	2.94	87.71	2.79	-	6.56	2.94
D	-	33.70	3.40	-	-	0.2
E	0.73	86.77	12.49	-	-	-

An analysis of EDS shows that the intermetallic compounds (marked as arrow A) in Figure 3a reveals that a Chinese-script-like compound appears in the microstructure has a typical composition of the π-AlFeSiMg phase which shows up grey under optical microscope. Figure 3b showed the needle-like bright phase (arrow B) believed to be the β-(Al_5FeSi) phase, which shows up light grey under an optical microscope. Figure 3c shows that the white contrast (arrow C) has a typical composition of the Al_2Cu phase. Figure 3d shows the typical microstructure of the Al_3Ti phase in the Al matrix (arrow D). Figure 3e shows the Mg_2Si phase (arrow E). When the alloying element is added to the molten alloy, a portion of element dissolves in the matrix while the undissolved portion forms compounds with other elements in the aluminium matrix. The solubility of the elements in aluminium alloys decreases with decreasing temperature. As the concentration of high alloying elements in the matrix decreases at high temperatures, low-concentration metal compounds are formed during the solidification process.

3.2. Rheocasting of A356 Alloy

The first technique used in this study to modify the microstructure of the A356 alloy is rheocasting using cooling-slope. Several methods were used to produce a feedstock with a spherical microstructure. Cooling-slope is a simple and fast technique for producing billets with a globular shape in comparison to other methods. In this method, an electrical furnace was used to melt the alloy, and then the molten alloy was poured into the mould via the inclined water-cooling plate. In addition to the pouring temperature, the length and width of the cooling-slope are important parameters that determine the formation of a microstructure with a smaller and predominantly spherical primary α-Al phase. The spherical microstructure is a requirement of the thixoforming processing and affects the alloy properties [22,23].

Microstructural Evaluation of Cooling-Slope A356 Alloy

The optical micrographs in Figure 4 show the low and high magnifications of the cooling-slope A356 alloy poured at 620 °C on a 250 mm-long cooling-slope plate with a 60° tilt angle, based on our previous work [9,20]. The α-Al dendrite structure in the as-cast alloy is completely transformed into a nearly spherical and rosette-like morphology with an average size of 53.6 μm that is surrounded by a coarse eutectic phase. When the molten metal was poured onto a cooling-slope, the molten alloy temperature dissipated followed by the abrupt temperature drop below the liquidus temperature. It was possible for a partial coagulation of the α-Al phase to take place on the cooling-slope.

The primary α-Al phase was detached as a result of the shear action, trapped in the flowing melt, and collected in the mould before it grew into dendritic shape. Shear stress is imposed on the melt as it flows down the plate due to gravitational force, and this eventually resulted in the breaking of the dendritic arms growing on the plate and transformed the plate α-Al phase into a rosette-like microstructure, which finally became almost spherical [24]. Nevertheless, a portion of the rosette microstructures lacks sufficient duration for achieving a fully globular form, as illustrated in Figure 4a.

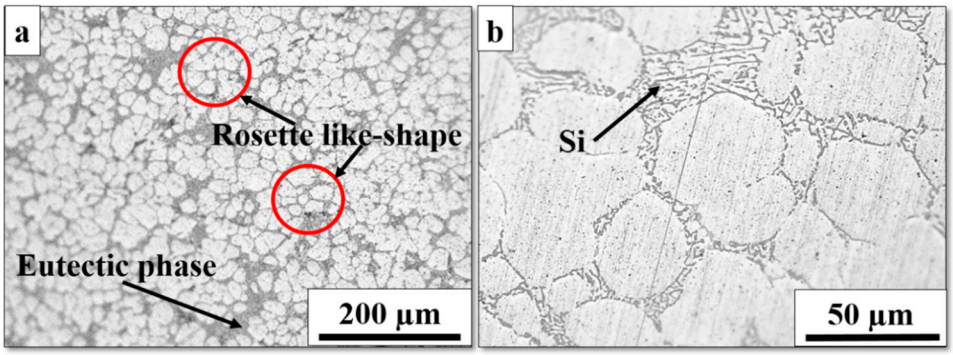


Figure 4. Optical micrographs of cooling-sloped of the A356 alloy at (**a**) low and (**b**) high magnification.

The flake-like shape of the eutectic Si particles transformed into a fine lamellar shape as shown in Figure 4b. After pouring the molten alloy, the heat transfers from the molten upon contact with the surface of the cooling plate reduces solidification time and shear effects [25]. Compared to the as-cast alloy, the α-Al microstructure surrounded by a eutectic phase is more uniformly distributed in the rheocasting alloy. An earlier study has shown that cooling-slope process produced refined Si particles [8]. In Figure 5a, a SEM micrograph is shown of flaky eutectic Si particles with an average size of 4.2 µm. Figure 5b shows the change in the eutectic Si morphology of the cooling-slope sample into a mixture of a lamellar and relatively spheroid shape, which is indicated by the red circle, with an average size of 3.01 µm.

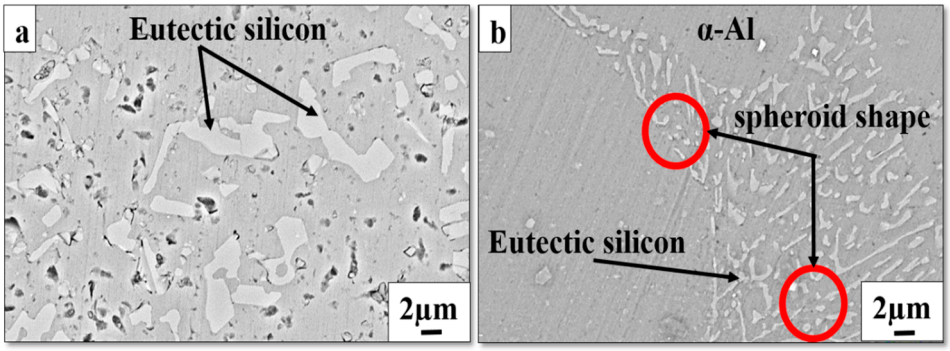


Figure 5. SEM micrographs of Si particles of the (**a**) as-cast and (**b**) cooling-sloped A356 alloy.

3.3. Heat Treatment of A356 Alloy

The second technique employed in this study in an attempt to modify the microstructure of the A356 alloy is heat treatment. The primary reason for applying heat treatment is to refine the eutectic phase in the A356 alloy. T6 heat treatment has three steps, solution heat treatment, rapid quenching, and artificial ageing treatment.

Microstructural Evaluation after Heat Treatment

The A356 alloy is a hypoeutectic Al–Si alloy that can be heat treatable. Figure 6a,b show the optical microstructures of the A356 alloy before and after T6 heat treatment, respectively, while Figure 6c,d are high-magnification optical micrographs of Si particles before and after T6 heat treatment. The flaky morphology of Si particles in the T6 heat-treated as-cast samples was transformed to spherical-shaped with a considerable amount lamellar shaped particles remaining after the T6 heat treatment process Figure 6b,d. The eutectic Si particles are refined and have fewer sharp edges than the as-cast alloy before heat treatment. The eutectic Si particles are broken up and spheroidised during the coarsening stage in solution treatment [10,26–28].

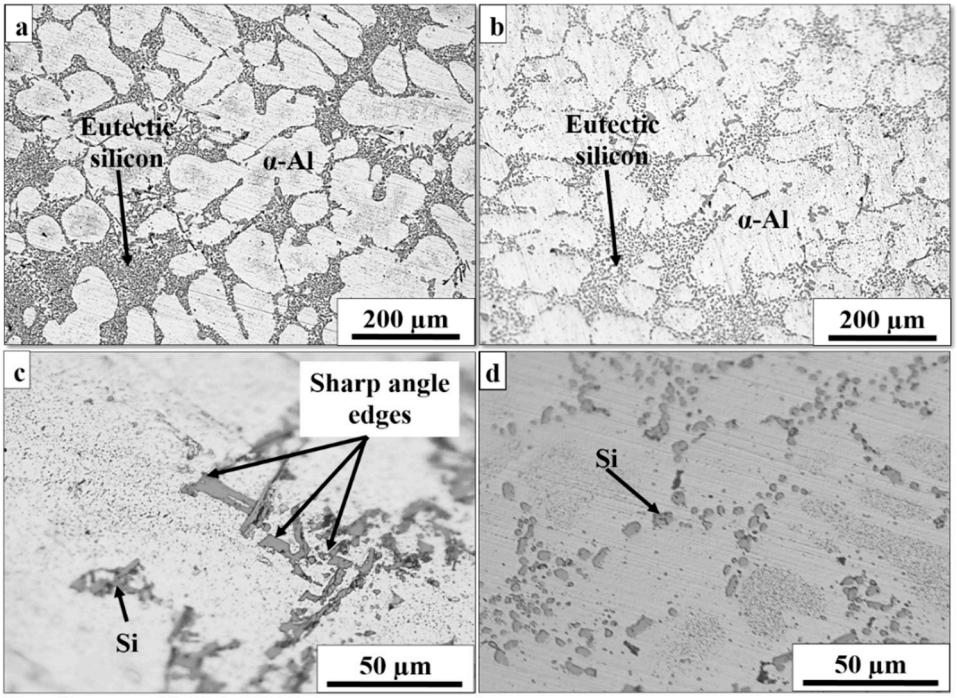


Figure 6. Optical micrographs of as-cast A356 alloy (**a**) before T6 heat treatment, (**b**) after T6, high magnification of Si particles, (**c**) before T6, and (**d**) after T6 treatment.

The T6 solution heat treatment had an impact on the morphology of the Si particles; the initial small size of eutectic Si particles is agglomerated by the Si diffusion mechanism in the aluminium matrix. The diffusion of eutectic Si is facilitated by the temperature increase, which promotes the growth of Si crystals into a more spheroidised shape and more homogenised in the Al matrix [29]. The eutectic Si particles of the untreated alloy become spheroidised and coarser after the T6 solution heat treatment, as shown in the SEM micrographs in Figure 7. The spheroidisation and coarsening of the eutectic Si was due to the elevated temperature in the T6 heat treatment. The Si particles of the as-cast sample gradually transformed from having a sharp edge into rounder and stubbier particles and formed necking while still remaining interconnected. The flake and acicular eutectic Si particles in the unmodified structure started to disintegrate into smaller fragments and gradually spheroidised. The transformation of the shape and size of eutectic Si particles during T6 solution heat treatment occurs in three stages. In the first stage, the Si particles undergo necking and fragmentation which reduce the size of Si particles due to the temperature rising. Spheroidisation takes place in the second stage, while in the third stage, Si particles that were broken up become coarser. The distribution of eutectic Si in as-cast, cooling-slope alloys at room temperature is affected by solution treatment. The eutectic Si in cooling-slope is much more evenly distributed than in the as-cast samples [30]. Table 2 presents the result of the quantitative metallography evaluation of the microstructures' attributes and after the T6 treatment.

Table 2. Average size of Si particles.

Samples	Si Size (µm)
As-cast	4.2 ± 0.8
T6 heat-treated as-cast	2.5 ± 0.4
Cooling-slope	3.0 ± 0.5
T6 heat-treated cooling-slope	2.3± 0.4

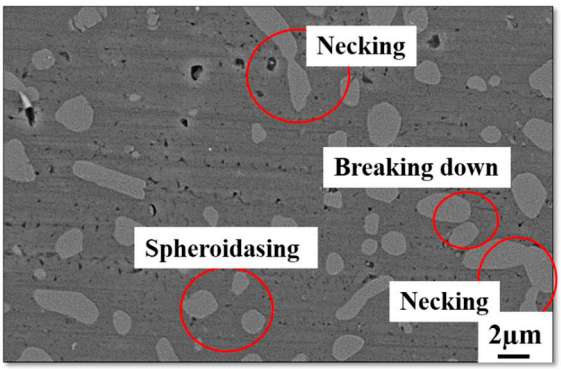


Figure 7. SEM micrograph of spheroidised and coarse eutectic Si particles after T6 heat treatment of the A356 alloy.

3.4. Evaluation of Cooling-Slope and Heat Treatment Process on Hardness of A356 Alloys

In Figure 8, the average Vickers microhardness of the A356 alloy samples in their as-cast and semi-solid states before and after T6 heat treatment are shown. The increase in hardness of the alloy after cooling bevel processing can be traced to the microstructural change from coarse dendrites of α-Al to a spherical shape accompanied by changes in Si particle size and morphology, as well as structural homogeneity. As indicated in Table 3, the alloy hardness increased from 61 to 83 HV after the cooling-slope process. Shear force can break the dendrite arms of the α-Al phase, leading to the refinement of the alloy grain. As a result, in the cooling-slope condition, the microstructure becomes smaller and denser. When compared to the as-cast sample, the microstructure of the rheocast sample possesses the maximum microhardness [31]. In the cooling-slope samples, the Si particles transformed into either lamellar or acicular shapes. This transformation significantly improved the microhardness of the A356 alloy. After T6 heat treatment, eutectic Si is spheroidised, leading to a hardness increase. The ultimate tensile strength and hardness of the A356 alloy are typically increased by the spheroidisation of Si particles during T6 heat treatment and the precipitation of magnesium silicide (Mg_2Si) particles during the ageing process [7,32].

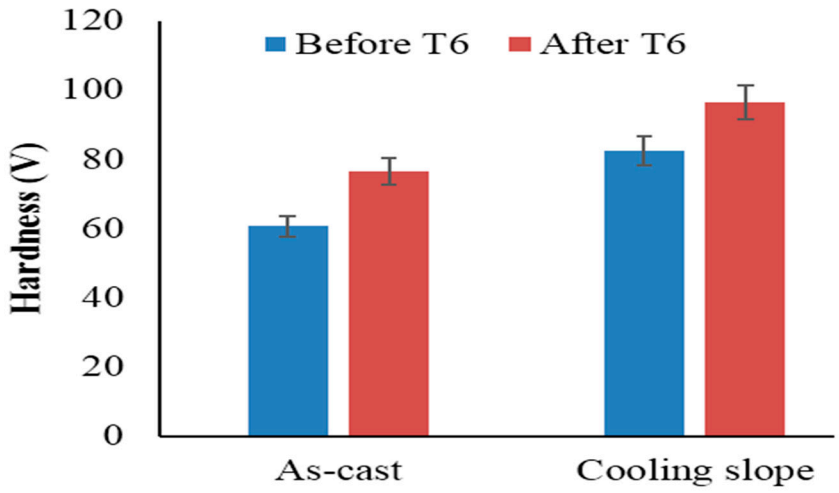


Figure 8. Microhardness of as-cast and cooling-slope A356 alloy before and after T6.

3.5. Equal Channel Angular Pressing of A356 Alloy

An (SPD) procedure using (ECAP) by route A is the third technique employed in the current work to refine the microstructure of as-cast and cooling-slope samples of the A356 alloy before and after heat treatment.

Table 3. Average of microhardness.

Samples	Microhardness (HV)
As-cast	61
T6 heat-treated as-cast	77
Cooling-slope	83
T6 heat-treated cooling-slope	97

3.5.1. ECAPed Microstructure of As-Cast

Figure 9a,b, respectively, show the microstructure of the as-cast and heat-treated as-cast samples following two ECAP passes via route A.

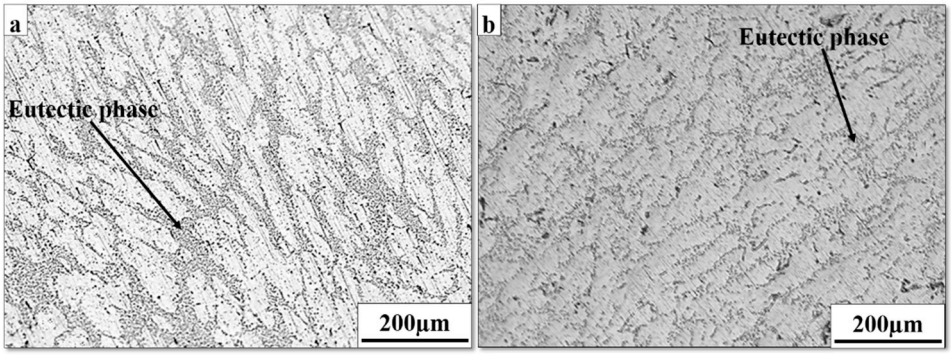


Figure 9. Optical micrographs of ECAPed (**a**) as-cast and (**b**) heat-treated as-cast A356 alloy after two ECAP passes by route A.

The primary Al grains in the A356 alloy were elongated after two ECAP passes, with varying lengths, and the grain boundaries were likely oriented at a 45° angle. The eutectic phase was irregularly distributed throughout the matrix, and the microstructure was somewhat inhomogeneous. The second ECAP pass significantly reduced the initial grain sizes of the as-cast and heat-treated as-cast samples from roughly 170.5 µm to approximately 105.1 and 62.9 µm, respectively.

The optical micrographs in Figure 10a,b show the low and high magnifications of ECAPed as-cast A356 alloy samples after four ECAP passes by route A. The application of greater strain by route A caused the primary α-Al phase and eutectic phase to be elongated into a plate-like shape in the as-cast sample before and after T6 heat treatment. The primary α-Al phase and the eutectic phase become finer after four ECAP passes as shown in Figure 10a,b. This finding aligns with the research conducted by [33,34]. Figure 10c,d show the microstructure of the as-cast and cooling-slope samples after four passes by route A. The primary α-Al changed morphologically from a dendritic to a longitudinal shape, while Table 4 shows how the ECAP processing using route A caused disintegration of the Si particles from large flakes to evenly sized fragments along the grain boundaries. The modification of the α-Al phase and eutectic mixture phase were the two significant effects observed in the microstructure of the A356 alloy after the ECAP process. ECAP processing by route A fragmented the flaky coarse Si to small particles with an-average size of approximately 1.0 µm after four ECAP passes by route A. The size of the grains of the ECAPed as-cast alloy reduced from 170.5 µm to 47.1 µm after four ECAP passes due to the dislocation density. Heat-treated as-cast A356 alloy subjected to ECAP processing shows a finer microstructure, where the α-Al grains and eutectic Si particle size are decreased to 0.4 and 0.76 µm, respectively. The samples processed by route A, on the other hand, are subjected to continuous shearing on only two crystallographic planes [35].

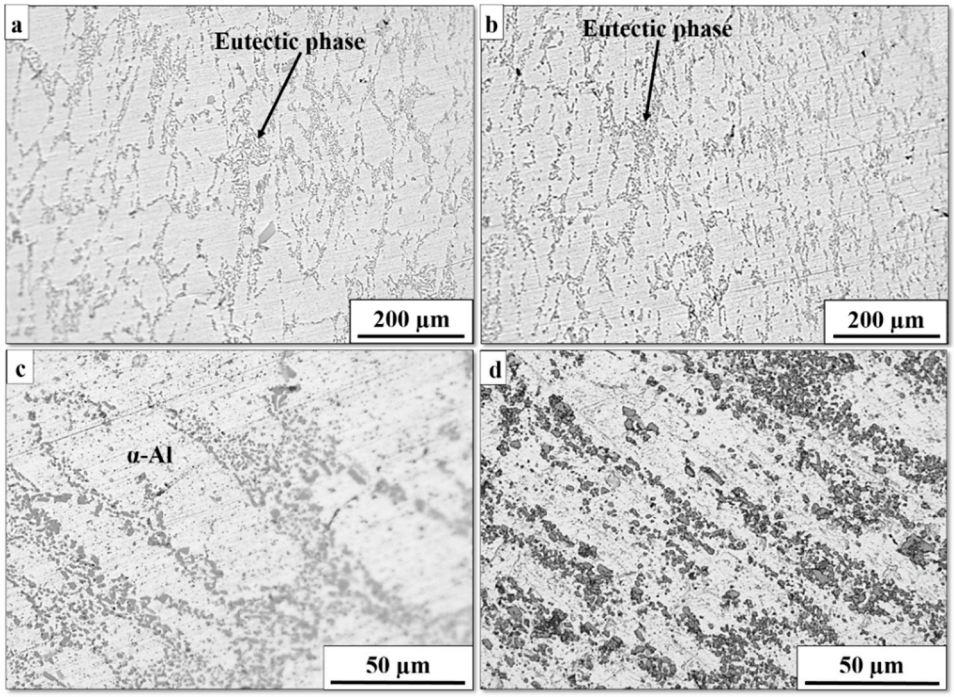


Figure 10. Different magnification of optical micrographs of ECAPed as-cast A356 alloy samples after four ECAP passes by route A of (**a**,**c**) as-cast and (**b**,**d**) heat-treated as-cast.

Table 4. Average size of the α-Al grain and Si particles of ECAPed as-cast A356 alloy.

Pass. Number	Si Particles Size (µm)	Grain Size (µm)
As-cast, 2 pass	2.7 ±0.8	105.1
Heat-treated as-cast, 2 pass	1.7 ±0.6	62.9
As-cast, 4 pass	1.0 ±0.5	47.1
Heat-treated as-cast, 4 pass	0.8 ± 0.5	40.4

3.5.2. ECAPed Microstructure of Cooling-Slope

The optical micrographs in Figure 11 show the ECAPed heat-treated cooling- slope sample after two ECAP passes by route A. After two ECAP passes, the α-Al phase grains deformed into an elongated shape as shown Figure 11a. The second pass produced finer α-Al grains with a longitudinal shape as a result of the shear strain imposed as can be seen in Figure 11b. The microstructure shows the longitudinal shape of the α-Al grains enclosed with a eutectic phase, where the sizes of the α-Al grains and eutectic Si particles are decreased to 42.6 and 0.9 µm, respectively. The acicular morphology of Si particles in the cooling-slope microstructure are fragmented to a few micrometres in size due to the strain imposed within the sample.

The optical micrographs in Figure 12a,b show an ECAPed heat-treated cooling- slope sample A356 alloy after four and six ECAP passes by route A. The four ECAP passes produced finer α-Al grains with a fibrous-like shape as shown in Figure 12a, while the six ECAP passes produced a fine fibrous-like morphology. The α-Al phase grains are much more refined in the ECAPed heat-treated cooling-slope after six passes compared to four ECAP passes as shown in Figure 12b. Both ECAPed heat-treated cooling-slope-cast alloy samples showed fine Si particles and a eutectic phase after four and six ECAP passes. The microstructure refinement of the ECAPed cooling-slope samples are the result of the T6 heat treatment process in addition to Si fragmentation during the ECAP process as presented in Table 5.

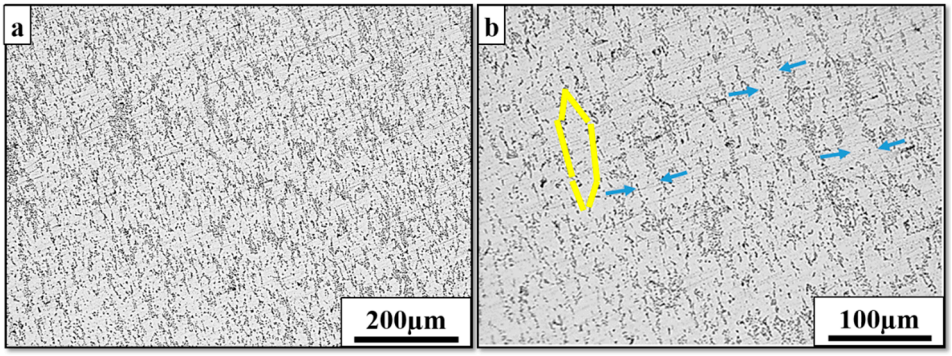


Figure 11. Optical micrographs of ECAPed heat-treated cooling-slope sample (**a**) after two ECAP passes by route A and (**b**) an enlarged image sample, the blue arrows show an example of α-Al grains (an example of which is highlighted yellow).

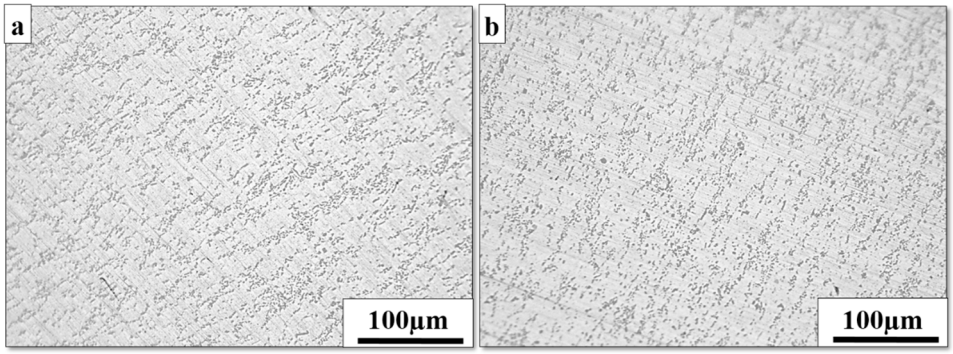


Figure 12. Optical micrograph of ECAPed heat-treated cooling-sloped samples after (**a**) four ECAP passes and (**b**) six ECAP passes.

Table 5. Average size of the α-Al grain and Si particles of ECAPed heat-treated as-cast and cooling-slope samples by route A.

Pass. Number	Si Particles (µm)	Grain Size (µm)
0 pass	4.2 ±0.48	170.5
Heat-treated cooling-slope, 2 pass	0.9 ±0.56	42.6
Heat-treated cooling-slope, 4 pass	0.74 ±0.46	29.3
Heat-treated cooling-slope, 6 pass	0.7 ± 0.22	23.1

3.6. Effect of Combining Heat-Treatment Semi-Solid Samples and ECAP Process on the Microstructure of A356 Alloy

The optical and SEM micrographs in Figure 13a–d show the micrographs after two passes by route A of the ECAPed heat-treated as-cast and cooling-slope A356 alloy samples.

The dendritic morphology of primary α-Al became elongated in the as-cast and cooling-slopes sample after two passes by route A, as can be seen in the optical micrograph in Figure 13a,c. The eutectic Si particles of as-cast and cooling-slope samples are fragmented and surround the α-Al phase after two ECAP passes as shown in the SEM micrograph in Figure 13b,d. The large coarse Si particles in the A356 alloy samples are further fragmented after the second pass, the grains size of the as-cast and cooling- slope alloy samples are markedly reduced from their initial value of ~170 µm to ~62.9 and 42.6, respectively. Tables 4 and 5 illustrates the fragmentation of the Si particles with increasing ECAP passes. At the end of the two ECAP passes conducted in the current study, the microstructure shows an elongated α-Al shape but still remains inhomogeneous.

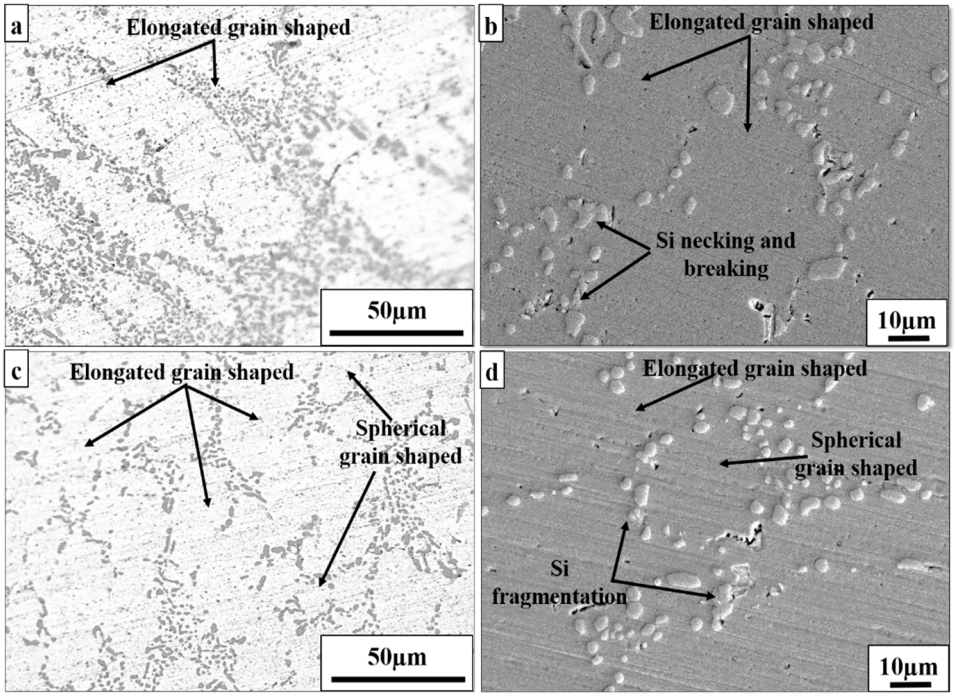


Figure 13. Optical and SEM micrograph of ECAPed heat-treated (**a**,**b**) as-cast and (**c**,**d**) cooling-sloped A356 alloy samples after two ECAP passes by route A.

Figure 14a,b show the SEM micrograph of the ECAPed heat-treated as-cast and cooling-slope A356 samples after four ECAP passes by route A. The primary α-Al and eutectic constituent phases of both the ECAPed as-cast and cooling-slope alloy samples are elongated after four ECAP passes. Figure 14c shows a micrograph of the ECAPed heat-treated cooling-slope A356 alloy samples after six ECAP passes via route A. The size of Si particles is further fragmented at large strains, and the particles are more homogeneously distributed within the banded regions after six ECAP passes, as can be seen in Figure 14c, Tables 4 and 5.

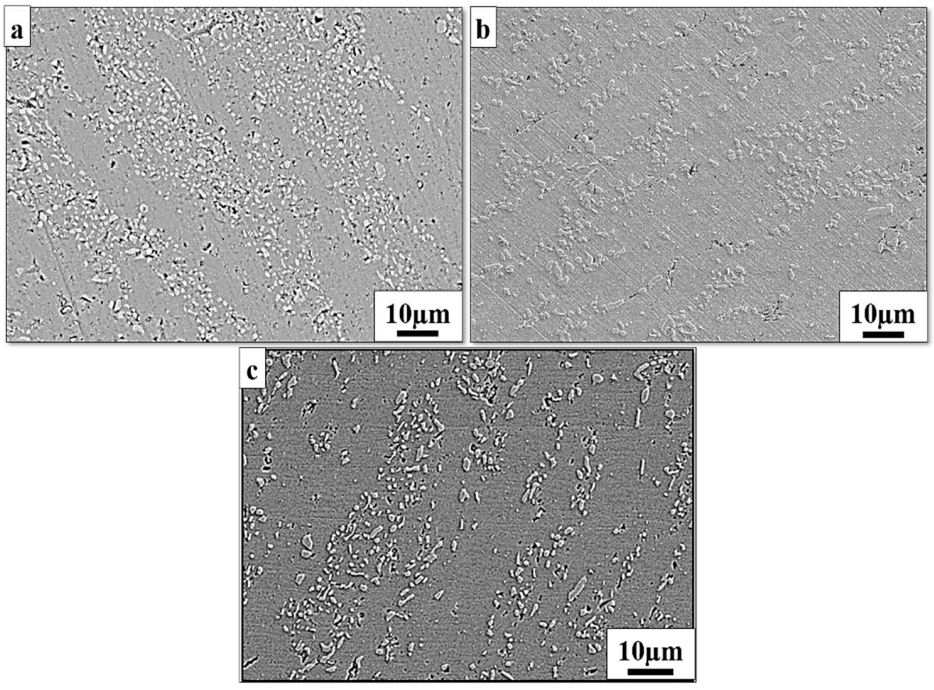


Figure 14. SEM micrograph of ECAPed heat-treated (**a**) as-cast, (**b**) cooling-sloped after four passes, and (**c**) heat-treated cooling-slope after six ECAP passes.

Figure 15a,b show the higher-magnification SEM micrographs of eutectic Si particles in the ECAPed heat-treated cooling-slope after four and six passes, respectively. Si particles continue to be fragmented with a greater number of ECAP passes, as can be seen in Figure 15c.

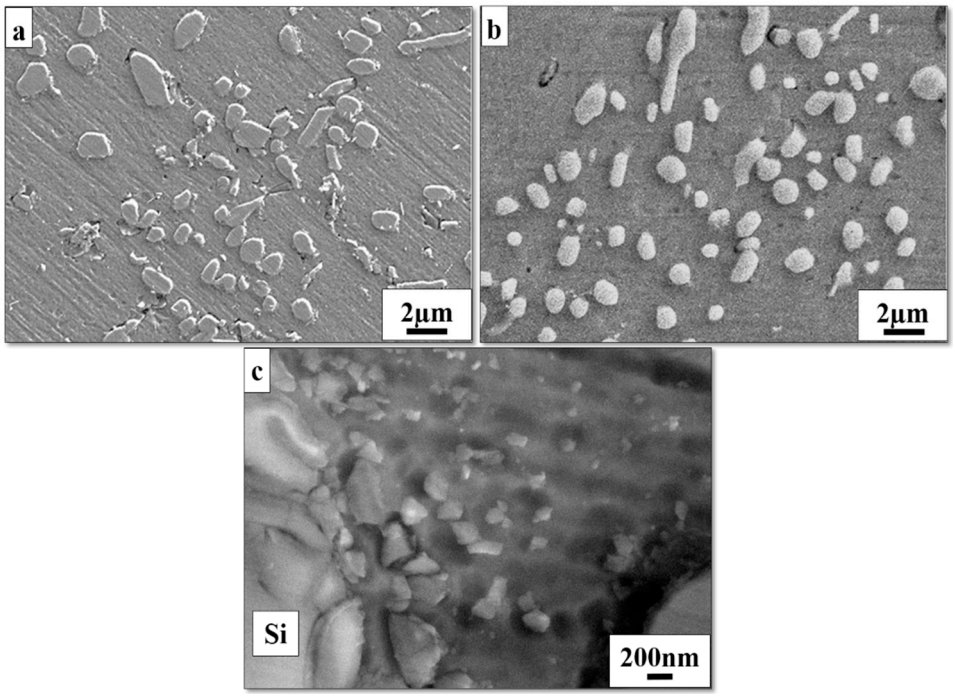


Figure 15. SEM micrograph of Si particles of (**a**) ECAPed heat-treated cooling-sloped after four passes, (**b**) after six passes, (**c**) Si particles fragmentation during ECAP processing.

The FETEM micrograph shows highly deformed grains after six ECAP passes of heat-treated cooling-slope. As shown in Figure 16, the formation of many dislocations and subgrains can be seen and a significant reduction in the α-Al grains' size.

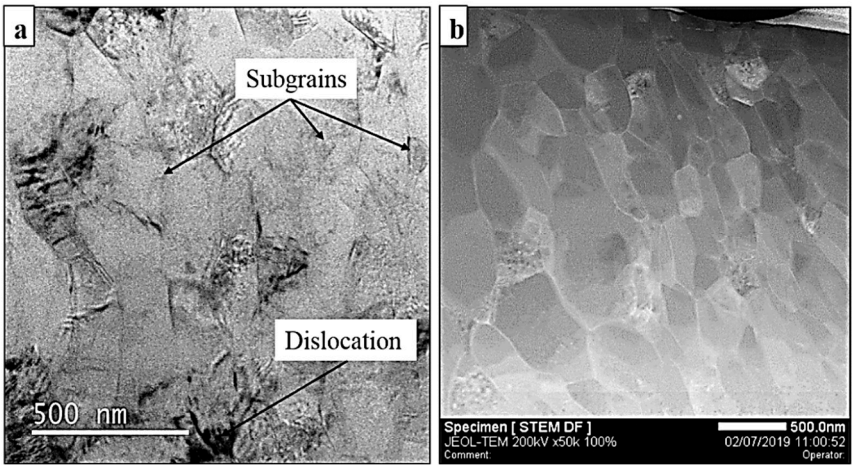


Figure 16. TEM micrograph of an ECAPed heat-treated cooling-slope sample (**a**) subgrains and (**b**) grain refinement.

The application of shear strain during ECAP processing leads to the accumulation of dislocations and the formation of cell structures with a significantly high dislocation density. The dislocations remain confined to the cell structures and do not affect the boundaries between cells or cause the formation of walls that divide them into smaller cells [36,37].

FETEM observation of ECAPed heat-treated cooling-slope samples after six passes confirms the presence of a high density of dislocations within the cell boundaries, subgrains with elongated shape, and ultra-fine grains. The grains are smaller than the average of the as-cast sample grain size.

3.7. Effect of Combining Heat-Treatment Semi-Solid Samples and ECAP Process on the Hardness of A356 Alloy

In Figure 17, the average Vickers microhardness of the as-cast and cooling-slope samples after undergoing ECAP processing via route A is presented. The microhardness increases with each ECAP pass. The hardness of the ECAPed heat-treated cooling-slope samples increases after two passes by route A, due to microstructure refining and fragmentation of eutectic Si particles. After four ECAP passes of the heat-treated as-cast and cooling-slope samples, the hardness rises from 61 HV to 125 and 129 HV, respectively. The ECAPed heat-treated cooling-slope sample achieve a microhardness of 134 HV after six passes. High strain induced after six ECAP passes increases the dislocation density, grain refinement, homogenization, and fragmentation of eutectic Si particles in the heat-treated cooling-slope samples. This leads to a significant improvement in hardness, which aligns with the findings of previous studies [33,38,39]. The heat-treated cooling-slope-cast sample features a homogenous distribution in the primary α-Al phase and the eutectic phase fragmentation.

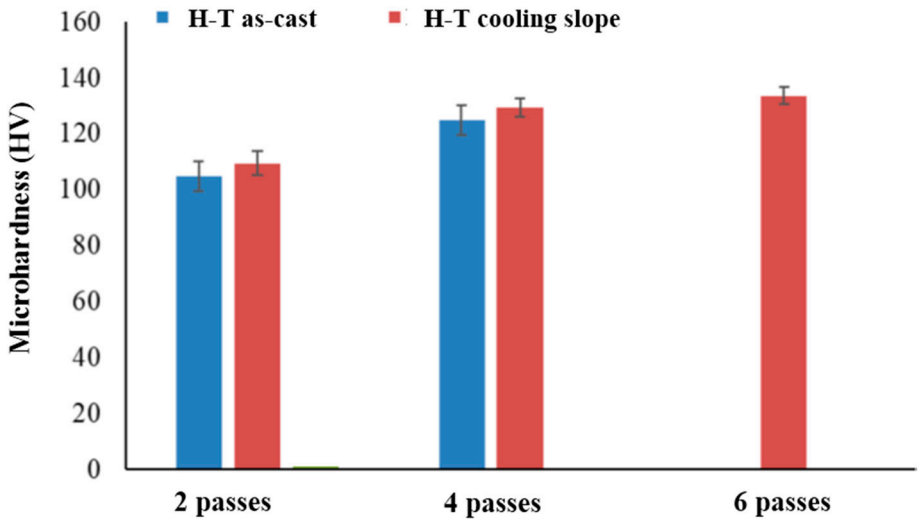


Figure 17. Microhardness of the ECAPed heat-treated (H-T) as-cast and cooling-slope samples by route A of the A356 alloy.

3.8. HPT Processing of A356 Alloy

The fifth grain refinement technique used in this study is the HPT process with different turns to investigate its effect on microstructure refinement, as well as its impact on hardness. Two sets of optical images were captured for the as-cast and cooling-slope samples before and after undergoing heat treatment through HPT. These images were taken at two distinct locations—at the centre of the disk (r = 0 mm) for both the as-cast and cooling-slope samples, and near the edge of the disk (r ≈ 3/4 R, where R is the radius of the disk) (Figure 1).

3.8.1. HPTed Microstructure of As-Cast and Cooling-Slope Using 0.75 Turn before and after T6

Figure 18 shows optical micrographs of both the centre and edge regions of the cooling-slope sample after 0.75 turns of HPT processing before T6 heat treatment. The optical micrograph of the centre and edge of the as-cast sample is shown in Figure 18a,b, where large grains of primary α-Al phase at the sample centre can be seen, while a longitudinally oriented α-Al phase at the sample's edge can be observed due to the applied strain. The unaltered shape of the α-Al phase in the as-cast sample at the centre may be attributed to

its original large size. On the contrary, Figure 19c,d show how the eutectic phase and Si particles at the edge are heterogeneously dispersed despite the relatively small size of the primary α-Al phase in the cooling-slope sample before HPT processing. The eutectic phase and Si particles of the as-cast and cooling-slope samples are heterogeneously distributed at the disk edge. The presence of the α-Al phase in the edge can be explained by the low shear strain resulting from a 0.75 turn. Consequently, there is a heterogeneous spread of Si particles, as illustrated in Figure 18b,d.

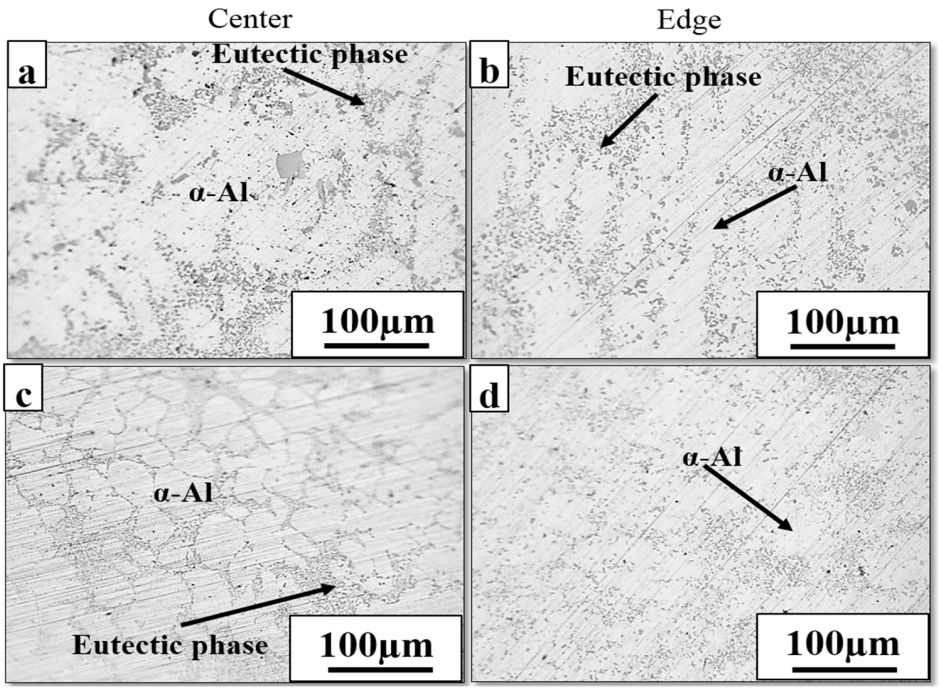


Figure 18. Optical micrographs of the centre and edge of HPTed (**a**,**b**) as-cast and (**c**,**d**) cooling- sloped A356 alloy after a 0.75 turn.

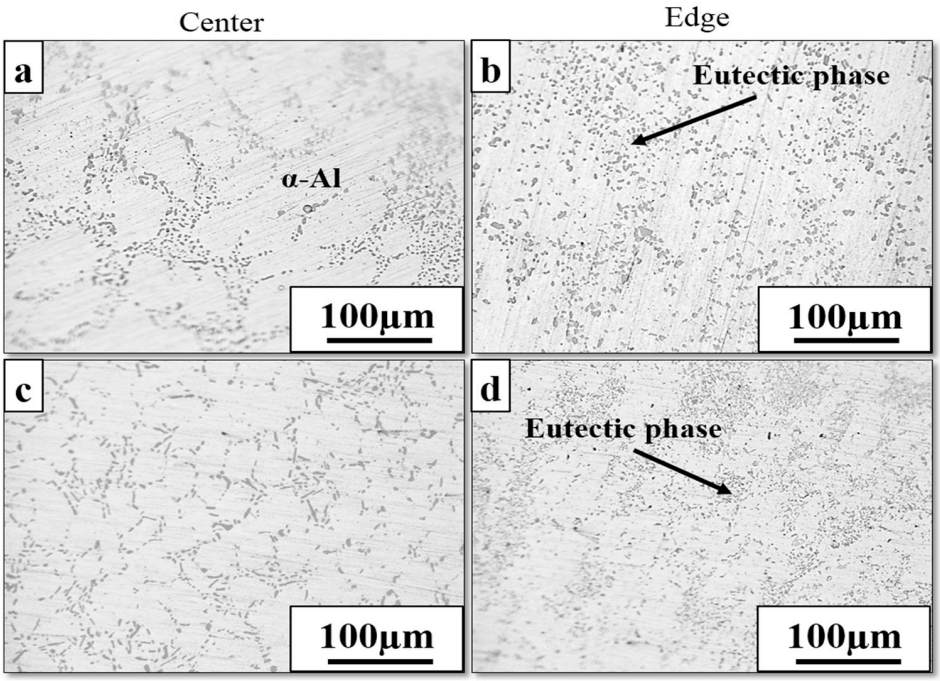


Figure 19. Optical micrographs of the centre and edge of HPTed heat-treated (**a**,**b**) as-cast and (**c**,**d**) cooling-slope A356 alloy after a 0.75 turn.

The microstructures of HPTed heat-treated as-cast and cooling-slope A356 alloy samples after a 0.75 turn are shown in Figure 19a–d. At the edge of the heat-treated as-cast and cooling-slope samples, the distribution of the Si particles and eutectic phase is heterogeneous.

3.8.2. HPTed Microstructure of As-Cast and Cooling-Slope Using Five Turns before and after T6

The mapping of the centre and edge of as-cast and cooling-slope A356 alloy after five turns of HPT processing with 6.0 GP applied pressure is shown in Figure 20. The α-Al phase is visible in the centre of the disk after HPT processing of the as-cast and cooling-slope samples, as shown in Figure 20a,c. Due to the increased number of turns, the grain boundaries of the primary α-Al phase are less visible at the edge due to greater shear. Figure 20b,d show that the Si particles are distributed homogeneously and uniformly. The homogeneous and uniform distribution of the Si particles is depicted in Figure 20b,d. In contrast to the cooling-slope alloy disk, the as-cast sample's disk edge has comparatively large eutectic Si particles. Both as-cast and cooling-slope samples have uniform eutectic Si particles within the aluminium matrix. However, the eutectic Si particles are broken into much smaller sizes, and the fraction of small Si particles is considerably higher. This aligns with the findings of [33] regarding microstructure homogeneity.

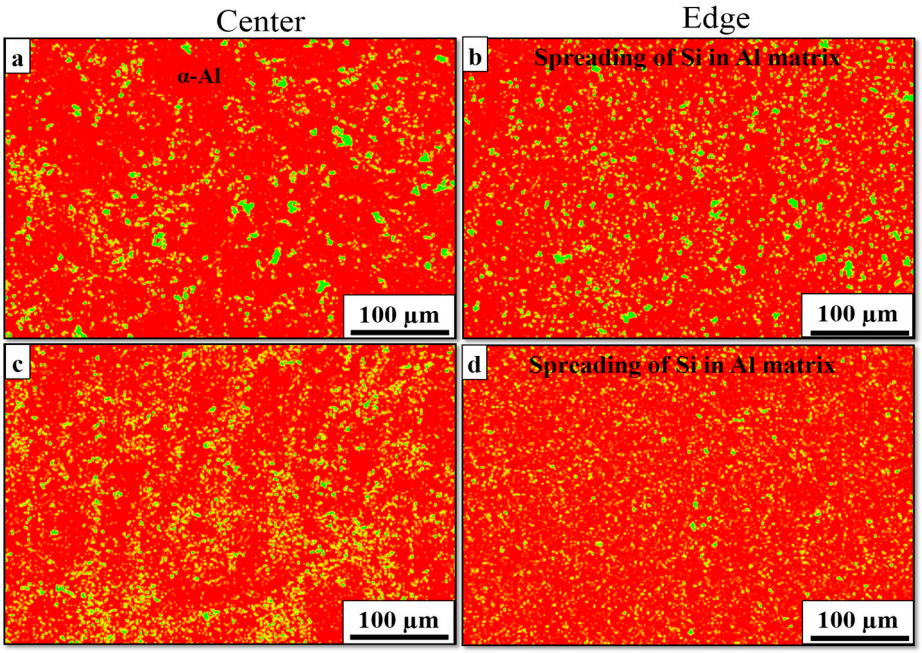


Figure 20. Mapping of Si particles in Al matrix at the centre and edge of HPTed (**a**,**b**) as-cast and (**c**,**d**) cooling-sloped A356 alloy after 5 turns.

Mapping of the centre and edge of HPTed heat-treated as-cast and cooling- slope A356 alloy samples under an applied pressure of 6.0 GPa after five turns is illustrated in Figure 21. After undergoing a combined heat treatment and semi-solid process, the samples displayed smaller Si particles, which were then fragmented by the HPT process due to high strain. The distribution of eutectic Si particles was more even in the cooling-slope samples than in the as-cast and untreated samples after five turns. The processed samples showed a finer microstructure at the edges due to greater torsional strain during HPT, as shown in Figure 21d.

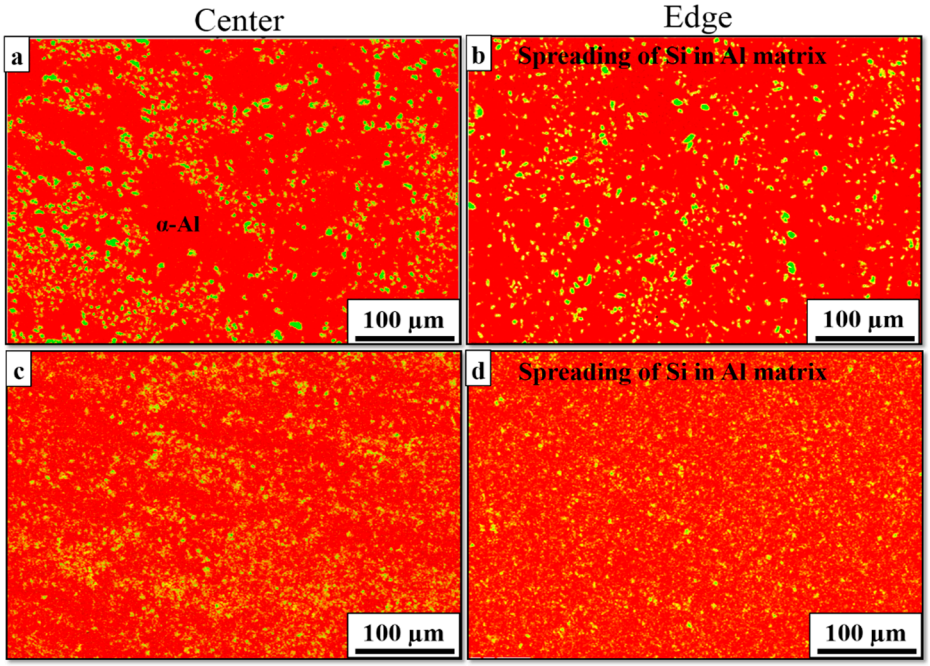


Figure 21. Mapping of Si particles in Al matrix at the centre and edge of HPTed heat-treated (**a**,**b**) as-cast and (**c**,**d**) cooling-sloped A356 alloy after 5 turns.

3.9. Effect of Combining Heat-Treatment Semi-Solid Samples and HPT Process on the Microstructure of A356 Alloy

The FETEM micrographs in Figure 22a represent heat-treated cooling-slope A356 alloys processed via HPT after five turns. Dislocations appeared within many grains after subjecting the sample to five turns, in particular near grain boundaries. The formation of the extra size grains (marked A) could be attributed to using Ga irradiation during ion milling. It is worth noting that employing Ga ions to perform ion milling at an energy of 30 keV for 180 min produces a marked recovery and smoother grain boundaries [40]. Figure 22a shows the dislocation cell structure (marked B) as a result of the intense plastic deformation that occurs in the HPT processing of heat-treated cooling-slope samples. The FETEM micrograph of the HPTed semi-solid A356 alloy exhibits a structure with considerable dislocation density. Dislocations can change position and interact with each other during shear deformation, forming a structure of dislocation cells that has a high dislocation density. Figure 22b shows that the microstructures are made up of sub-grains. Additional straining results in the formation of sub-grain boundaries due to the aggregation of dislocations. The micrographs show a noticeable decrease in grain size in terms of undeformed material. Previous studies have reported similar dislocation aggregation in semi-solid cast alloys [41]. Previous studies have shown that the high number of turns in HPT processing results in a high shear stress associated with a high dislocation density. This is due to grain refinement and increased strength [42–45].

The greater strain imposed by a higher number of turns in HPT processing gradually increases the misorientation until high-angle boundaries are eventually formed at immense strain [46,47]. As anticipated, the extensive dislocation is formed from the normal deformation mode, which then merges to produce the subgrains show in Figure 22. Higher strain produces smaller subgrains whilst increasing the dislocation density within the subgrains. An identical trend has been observed in Cu produced via HPT [48].

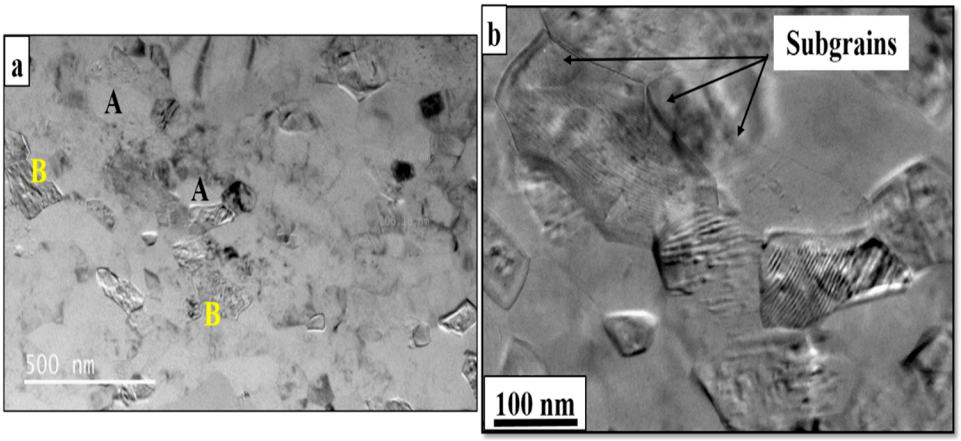


Figure 22. (**a**,**b**) TEM image of HPTed heat-treated cooling-sloped samples processed by HPT 5 turns.

Figure 23 shows that the HPTed heat-treated cooling-slope A356 alloy processed by five turns of the HPT process have distinct fine grains that have straight grain boundaries and high angles of misorientation, with an average grain size in the HPTed heat-treated cooling-slope sample of ~160 nm. Figure 23 shows less dislocation density in the grains after five HPT turns.

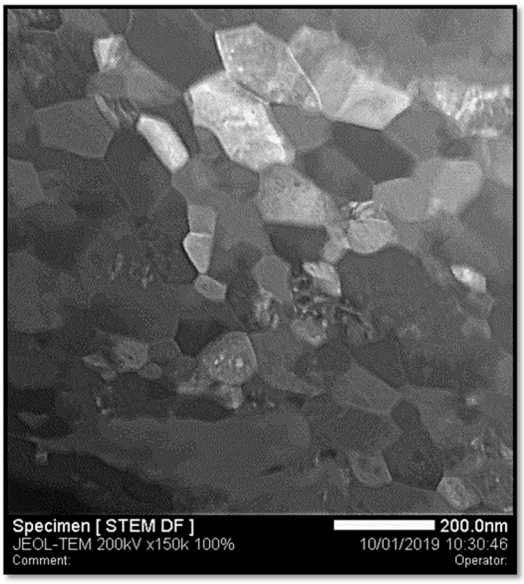


Figure 23. TEM micrographs of the HPTed heat-treated cooling-sloped grains after 5 turns of HPT.

The process of HPT resulted in grain purification, increasing the volume density of grain boundaries and inhibiting dislocation propagation, thereby strengthening the material. Figures 24 and 25 show the distribution of alloying elements and Si particles at the edge of the HPTed heat-treated as-cast and cooling-slope A356 alloy after five turns. T6 heat treatment transforms the initial flaky and acicular-shape Si particles in the as-cast, cooling-slope samples into finer globular particles. The applied high compression pressure and strain fragments the Si phase into smaller particles; a marked reduction in the size of Si and intermetallic particles is also observed. Figures 24 and 25 show that the homogenous distribution of refined Si particles and alloying elements in the edge of heat-treated cooling-slope alloy is more visible than in the as-cast alloy.

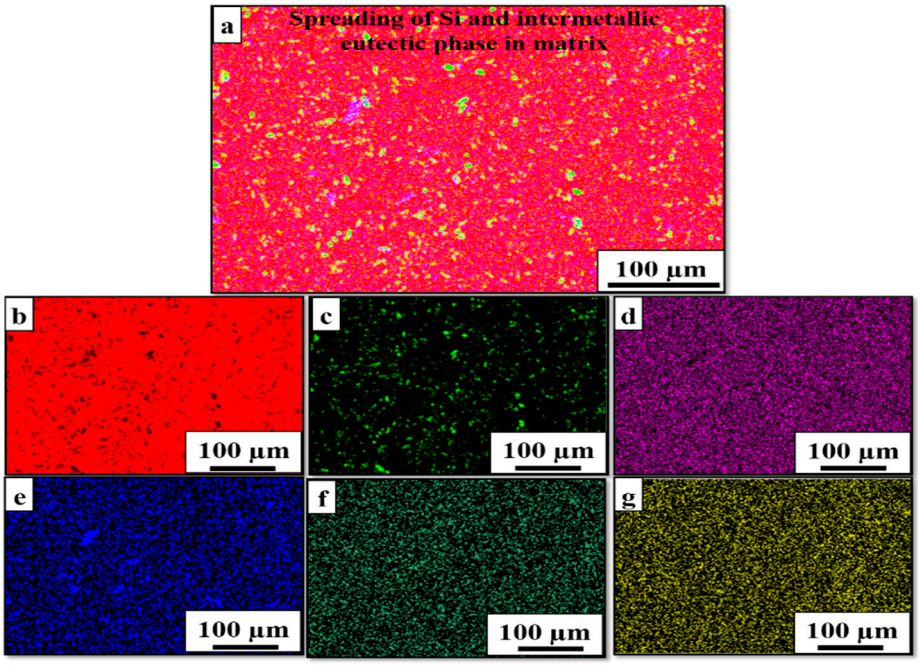


Figure 24. SEM-EDS mapping in the edge of the HPTed heat-treated as-cast sample (**a**) spreading of Si particles and intermetallic phases, (**b**) Al, (**c**) Si, (**d**) Mg, (**e**) Fe, (**f**) Ti and (**g**) Cu of A356 alloy.

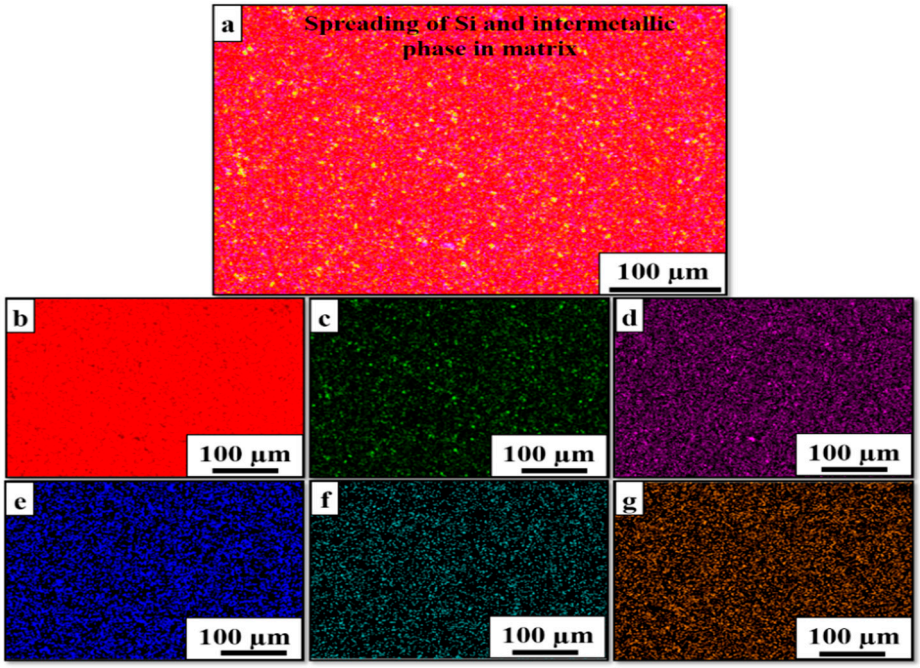


Figure 25. SEM-EDS mapping in the edge of the HPTed heat-treated cooling-slope sample (**a**) spreading of Si particles and intermetallic phases, (**b**) Al, (**c**) Si, (**d**) Mg, (**e**) Fe, (**f**) Ti, and (**g**) Cu of the A356 alloy.

These results indicate the profound impact of applying heat treatment to the acicular-like shape of Si particles prior to HPT processing on the final size and distribution of initial coarse Si particles. The alloying elements in the centre of the as-cast alloy are not homogenously distributed in comparison to the semi-solid samples due to the primary α-Al size at the centre. The spreading of alloying elements at the centre of the cooling-slope samples is homogenously distributed as shown in Figure 26.

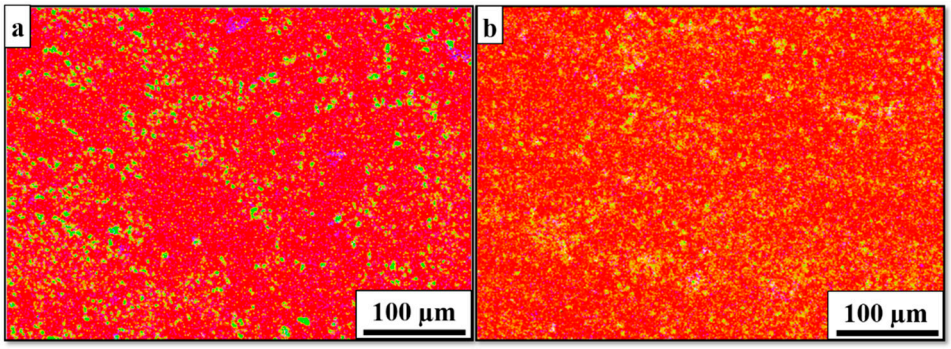


Figure 26. Mapping of alloying element and Si particles distribution in the centre of HPTed heat-treated, after 5 turns, (**a**) as-cast and (**b**) cooling-slope A356 alloy.

3.10. Effect of Combining Heat-Treated Semi-Solid Samples and HPT Process on the Hardness of A356 Alloy

In Figure 27a,b, the Vickers microhardness values of the A356 alloy disks were measured before and after T6 heat treatment at two different turning, 0.75 and 5 turns, and are displayed in the table. The hardness is measured at 0.5 mm intervals across each disk's diameter. The HPT process results in a significant improvement in hardness. It is important to note that the hardness increase is more pronounced at the disk's edge than at the centre. By subjecting the A356 cast alloy to the HPT process, its initial hardness is significantly increased. During the deformation process, the hardness values in the centre of the disks are initially low, but they rapidly grow with increasing applied strain. The hardness variability depends on the number of turns and the disk's position from the centre to the edge during HPT processing. Figure 27a shows the different microhardness values throughout the cross-section of the HPTed sample with the centre of the disk having the lowest microhardness value and gradually increasing towards the edge. In HPT processing, the strain increases as it approaches the edge of the disk and therefore the degree of deformation varies across the diameter of the sample. It is known that the mechanical properties are primarily determined by the condition of the microstructure. The low hardness values in the centre of the disk can be attributed to the retention of the primary α-Al phase; their initially large size due to the lack of shear strain in this area is shown in Figures 18–21 this is similar with the findings made by [49–51].

Figure 27a,b illustrate a more significant increase in hardness after 5 turns compared to 0.75 turn. According to Figure 27b, the hardness of the disk increases significantly from the centre to the edge. The presence of eutectic Si particles and intermetallic phase dispersed homogeneously throughout the disk, as well as grain refinement after five HPT turns, resulted in an increase in hardness. This is consistent with the microstructures shown in Figures 24–26 where the samples subjected to five turns have smaller eutectic Si particles and intermetallic phases that are more evenly distributed in comparison to the samples subjected to 0.75 via HPT processing. Early research has shown that when the HPT turn number increases, it leads to higher shear strains that are correlated with a greater dislocation density. This, in turn, can be specifically linked to grain refinement and the subsequent increase in microhardness [42,52–55]. Most of the disks exhibit the typical hardness gradation brought about by strain hardening behaviour [49], where hardness increases from the centre to the edge of the disk as the equivalent strain in HPT is increased.

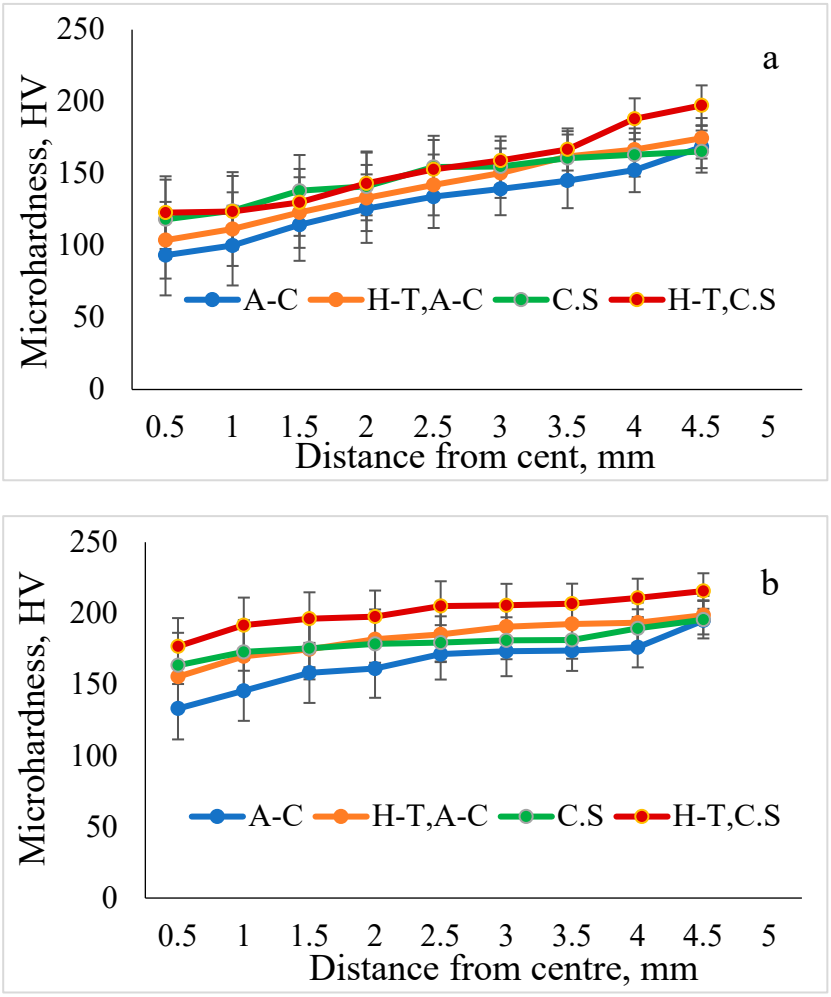


Figure 27. Microhardness of HPTed as-cast and cooling-sloped A356 alloy before and after heat treatment after (**a**) 0.75 and (**b**) 5 turns.

In summary, after the fourth pass of the heat-treated ECAP processing, the primary α-Al phase in the as-cast A356 alloy changed from a dendritic to longitudinal shape. The rough Si particles were broken down and spread along the boundaries of the α-Al phase. Table 4 clearly illustrates a reduction in the size of the α-Al phase reduced from 170 to 40.4 µm. Subjecting the as-cast alloy A356 to the cooling-slope process before severe plastic deformation resulted in the sample withstanding six ECAP passes, leading to an ultrafine microstructure and a significant improvement in hardness. After applying high-pressure torsion (HPT) processing to the cooling-slope samples, an ultra-fine microstructure with an average size of ~160 nm and a homogenous distribution of the eutectic phase in the Al matrix was obtained. It is clear that refining the microstructure through a semi-solid process before applying ECAP or HPT processing significantly improves microstructure refinement, as demonstrated by our previous publications [34,45]. Subjecting the fine microstructure to severe plastic deformation results in a higher level of refinement compared to applying the same technique to the dendritic structure, as shown in Tables 2–5 and Figures 20–25.

4. Conclusions

Commercial hypoeutectic A356 alloy was processed using different microstructural refining methods or a combination of these methods. The refined microstructural evaluations and their effect on hardness were studied. The following conclusions are based on the results of the study:

1. The dendritic morphology of the primary α-Al phase as-cast A356 alloy processed by semi-solid processing using the cooling-slope technique was replaced by a globules-like morphology. The lamellar or acicular-like-shaped Si particles were transformed into a fine acicular-like shape measuring 3.0 mm after cooling-slope. T6 heat treatment of the A356 alloy transformed the lamellar-like shape of Si particles in the cooling-slope microstructure into a spheroidised shape measuring 2.32 ± 0.42 µm. The hardness of the semi-solid A356 alloy after T6 heat treatment increased to 83 HV of the cooling-slope A356 alloy.
2. After undergoing four ECAP passes, the microstructure of the as-cast samples displayed an elongation of the primary α-Al phase and eutectic constituents, which resulted in fine plate-like shapes having an average size of 40.4 µm. Furthermore, the size of eutectic Si particles was reduced to 0.8 ± 0.47 µm. In contrast, the microstructure of the cooling-slope that underwent six ECAP passes after heat treatment showed a more uniform and finer distribution of α-Al grains and Si particles. Furthermore, the size of the Si particles decreased to 0.7 ± 0.22 µm. The alloy hardness increased from 61 HV to 125 and 129 HV after four passes of ECAPed heat-treated as-cast and cooling-slope samples. The sample heat-treated on the cooling-slope achieved the highest hardness value of 134 HV after undergoing six ECAP passes.
3. The A356 Al alloy was processed by HPT through 0.75 and 5 turns. As a result of the higher torsional deformation, there was a refinement of the microstructure and a homogeneous redistribution of intermetallic phase and Si particles in the Al matrix of the heat-treated cooling-slope samples. The grain size of the HPTed cooling-slope A356 alloy samples was reduced to 160 nm. The hardness of the HPTed heat-treated cooling-slope increased to 211 HV after five turns.

Author Contributions: Methodology, M.A.G.; Formal analysis, M.A.G.; Investigation, I.F.M., A.M.A. and O.M.I.; Writing—original draft, M.A.G.; Supervision, M.Z.O., I.F.M. and N.K.O. All authors have read and agreed to the published version of the manuscript.

Funding: This research received no external funding.

Institutional Review Board Statement: Not applicable.

Data Availability Statement: Not applicable.

Acknowledgments: The researchers would like to thank the Deanship of Scientific Research, Qassim University, for funding the publication of this project.

Conflicts of Interest: The authors declare no conflict of interest.

References

1. Haghdadi, N.; Zarei-Hanzaki, A.; Abedi, H.R.; Sabokpa, O. The effect of thermomechanical parameters on the eutectic silicon characteristics in a non-modified cast A356 aluminum alloy. *Mater. Sci. Eng. A* **2012**, *549*, 93–99. [CrossRef]
2. Davis, J.R. Aluminum and aluminum alloys. In *Light Metals and Alloys*; ASM International: Tokyo, Japan, 2001; Volume 66. [CrossRef]
3. Birol, Y. A357 thixoforming feedstock produced by cooling slope casting. *J. Mater. Process. Technol.* **2007**, *186*, 94–101. [CrossRef]
4. Haga, T.; Kapranos, P. Billetless simple thixoforming process. *J. Mater. Process. Technol.* **2002**, *130–131*, 581–586. [CrossRef]
5. Das, P.; Samanta, S.K.; Venkatpathi, B.R.K.; Chattopadhyay, H.; Dutta, P. Microstructural evolution of A356 Al alloy during flow along a cooling slope. *Trans. Indian Inst. Met.* **2012**, *65*, 669–672. [CrossRef]
6. Salleh, M.S.; Oma, M.Z.; AlhawariL, K.S.; Mohammed, M.N.; Ali, M.A.M.; Mohamad, E. Microstructural evolution and mechanical properties of thixoformed A319 alloys containing variable amounts of magnesium. *Trans. Nonferr. Met. Soc. China (Engl. Ed.)* **2016**, *26*, 2029–2042. [CrossRef]
7. Möller, H.; Govender, G.; Stumpf, W. Factors Influencing Testing Mechanical Properties of Al-7Si-Mg Alloys A356/7. *Light Metals* **2016**, *2012*, 467–471.
8. Nguyen, V.T.; Hussain, Z.; Anasyida, A.S.; Huy, T.D.; Almanar, I.P. Influence of Semi-Solid Casting and Equal Channel Pressing on Microstructure of a Hypoeutectic Al-Si Alloy. *Mater. Sci. Forum* **2015**, *819*, 9–14. [CrossRef]
9. Mohamed, A.M.A.; Samuel, F.H. A Review on the Heat Treatment of Al-Si-Cu/Mg Casting Alloys. *Conv. Nov. Appl.* **2012**, *1*, 55–72. [CrossRef]

10. Ogris, E.; Wahlen, A.; Lüchinger, H.; Uggowitzer, P.J. On the silicon spheroidization in Al-Si alloys. *J. Light Met.* **2002**, *2*, 263–269. [CrossRef]
11. Moradi, M.; Nili-Ahmadabadi, M.; Heidarian, B. Improvement of mechanical properties of AL (A356) cast alloy processed by ecap with different heat treatments. *Int. J. Mater. Form.* **2009**, *2*, 85–88. [CrossRef]
12. Wang, Q.G.; Praud, M.; Needleman, A.; Kim, K.S.; Griffiths, J.R.; Davidson, C.J.; Cáceres, C.H.; Benzerga, A.A. Size effects in aluminium alloy castings. *Acta Mater.* **2010**, *58*, 3006–3013. [CrossRef]
13. Garcia-Infanta, J.M.; Zhilyaev, A.P.; Cepeda-Jiménez, C.M.; Ruano, O.A.; Carreño, F. Effect of the deformation path on the ductility of a hypoeutectic Al–Si casting alloy subjected to equal-channel angular pressing by routes A, BA, BC and C. *Scr. Mater.* **2008**, *58*, 138–141. [CrossRef]
14. Gebril, M.A.; Omar, M.Z.; Mohamed, I.F.; Othman, N.K.; Abdelgnei, M.A.H. Corrosion improvement and microstructure evaluation of SEM-solid A356 alloy by ecap process. In Proceedings of the Journal of Physics: Conference Series, Penang, Malaysia, 12–13 December 2018; Volume 1082, p. 12110.
15. Gebril, M.A.; Omar, M.Z.; Mohamed, I.F.; Othman, N.K. Microstructural Evaluation and Corrosion Resistance of Semisolid Cast A356 Alloy Processed by Equal Channel Angular Pressing. *Metals* **2019**, *9*, 303. [CrossRef]
16. Ishak, N.N.M.; Salleh, M.S.; Yahaya, S.H.; Mohamad, E.; Sulaiman, M.A. The Effect of Equal Channel Angular Pressing (ECAP) on the Microstructure and Hardness of A356 Aluminium Alloy. *J. Adv. Manuf. Technol.* **2017**, *11*, 47–58.
17. Ashouri, S.; Nili-Ahmadabadi, M.; Moradi, M.; Iranpour, M. Semi-solid microstructure evolution during reheating of aluminum A356 alloy deformed severely by ECAP. *J. Alloys Compd.* **2008**, *466*, 67–72. [CrossRef]
18. Natori, K.; Utsunomiya, H.; Tanaka, T. Improvement in formability of semi-solid cast hypoeutectic Al-Si alloys by equal-channel angular pressing. *J. Mater. Process. Technol.* **2017**, *240*, 240–248. [CrossRef]
19. Nomura, F.; Matsuba, T.; Tanaka, T.; Imaida, Y. Improvement of mechanical properties of semi-solid alloys by ECAP processing. *Adv. Mater. Res.* **2010**, *123*, 483–486. [CrossRef]
20. Van Thuong, N.; Zuhailawati, H.; Seman, A.A.; Huy, T.D.; Dhindaw, B.K. Microstructural evolution and wear characteristics of equal channel angular pressing processed semi-solid-cast hypoeutectic aluminum alloys. *Mater. Des.* **2015**, *67*, 448–456. [CrossRef]
21. Samsudin, M.; Omar, M.Z.; Abdullah, S. Effects of rheocasting and thixoforming on the microstructure and mechanical properties of A356 aluminium alloy. *J. Teknol.* **2016**, *78*, 107–113. [CrossRef]
22. Rooy, E.L.; Linden, J.H.L. Van ASM Metals Handbook, Vol 02 Properties and Selection: Nonferrous Alloys and Special-Purpose Materials. 1990. Available online: http://sme.vimaru.edu.vn/sites/sme.vimaru.edu.vn/files/volume_2_-_properties_and_selection_nonf.pdf (accessed on 30 August 2023).
23. El-Mahallawi, I.S.-E.; Mahmoud, T.S.; Gaafer, A.M.; Mahmoud, F.H. Effect of pouring temperature and water cooling on the thixotropic semi-solid microstructure of A319 aluminium cast alloy. *Mater. Res.* **2015**, *18*, 170–176. [CrossRef]
24. Taghavi, F.; Ghassemi, A. Study on the effects of the length and angle of inclined plate on the thixotropic microstructure of A356 aluminum alloy. *Mater. Des.* **2009**, *30*, 1762–1767. [CrossRef]
25. Flemings, M.C. Behavior of metal alloys in the semisolid state. *Metall. Trans. B* **1991**, *22*, 269–293. [CrossRef]
26. Motegi, T.; Tanabe, F.; Sugiura, E. Continuous casting of semisolid aluminium alloys. In *Materials Science Forum*; Trans Tech Publications Ltd.: Wollerau, Switzerland, 2002; Volume 396, pp. 203–208.
27. Ogris, E.; Lüchinger, H.; Uggowitzer, P.J. Silicon spheroidization treatment of thixoformed Al-Si-Mg alloys. In *Aluminium Alloys 2002: Their Physical and Mechanical Properties: Proceedings of the 8th International Conference ICAA8, Cambridge, UK, 2–5 July 2002*; Trans Tech Publications: Bäch, Switzerland, 2002; Volume 396–402, pp. 149–154. [CrossRef]
28. Tiryakioğlu, M. Si particle size and aspect ratio distributions in an Al-7%Si-0.6%Mg alloy during solution treatment. *Mater. Sci. Eng. A* **2008**, *473*, 1–6. [CrossRef]
29. Li, B.; Wang, H.; Jie, J.; Wei, Z. Effects of yttrium and heat treatment on the microstructure and tensile properties of Al-7.5Si-0.5Mg alloy. *Mater. Des.* **2011**, *32*, 1617–1622. [CrossRef]
30. Menargues, S.; Martín, E.; Baile, M.T.; Picas, J.A. New short T6 heat treatments for aluminium silicon alloys obtained by semisolid forming. *Mater. Sci. Eng. A* **2015**, *621*, 236–242. [CrossRef]
31. Gecu, R.; Acar, S.; Kisasoz, A.; Altug Guler, K.; Karaaslan, A. Influence of T6 heat treatment on A356 and A380 aluminium alloys manufactured by thixoforging combined with low superheat casting. *Trans. Nonferr. Met. Soc. China (Engl. Ed.)* **2018**, *28*, 385–392. [CrossRef]
32. Liao, B.; Park, Y.; Ding, H. Effects of rheocasting and heat treatment on microstructure and mechanical properties of A356 alloy. *Mater. Sci. Eng. A* **2011**, *528*, 986–995. [CrossRef]
33. Zhu, M. Effects of T6 heat treatment on the microstructure, tensile properties, and fracture behavior of the modified A356 alloys. *J. Mater.* **2017**, *36*, 243–249. [CrossRef]
34. Cepeda-Jiménez, C.M.; García-Infanta, J.M.; Zhilyaev, A.P.; Ruano, O.A.; Carreño, F. Influence of the supersaturated silicon solid solution concentration on the effectiveness of severe plastic deformation processing in Al–7wt.% Si casting alloy. *Mater. Sci. Eng. A* **2011**, *528*, 7938–7947. [CrossRef]
35. Venkatachalam, P.; Ramesh Kumar, S.; Ravisankar, B.; Thomas Paul, V.; Vijayalakshmi, M. Effect of processing routes on microstructure and mechanical properties of 2014 Al alloy processed by equal channel angular pressing. *Trans. Nonferr. Met. Soc. China (Engl. Ed.)* **2010**, *20*, 1822–1828. [CrossRef]

36. Azimi, A.; Tutunchilar, S.; Faraji, G.; Givi, M.K.B. Mechanical properties and microstructural evolution during multi-pass ECAR of Al 1100—O alloy. *J. Mater.* **2012**, *42*, 388–394. [CrossRef]
37. Meyers, M.A.; Mishra, A.; Benson, D.J. Mechanical properties of nanocrystalline materials. *Prog. Mater. Sci.* **2006**, *51*, 427–556. [CrossRef]
38. Goodarzy, M.H.; Arabi, H.; Boutorabi, M.A.; Seyedein, S.H.; Najafabadi, S.H.H. The effects of room temperature ECAP and subsequent aging on mechanical properties of 2024 Al alloy. *J. Alloys Compd.* **2014**, *585*, 753–759. [CrossRef]
39. Kumar, S.R.; Gudimetla, K.; Venkatachalam, P.; Ravisankar, B.; Jayasankar, K. Microstructural and mechanical properties of Al 7075 alloy processed by Equal Channel Angular Pressing. *Mater. Sci. Eng. A* **2012**, *533*, 50–54. [CrossRef]
40. Edalati, K.; Horita, Z.; Furuta, T.; Kuramoto, S. Dynamic recrystallization and recovery during high-pressure torsion: Experimental evidence by torque measurement using ring specimens. *Mater. Sci. Eng. A* **2013**, *559*, 506–509. [CrossRef]
41. Barekar, N.S.; Pradhan, R.; Dhindaw, B.K. Mechanism of microstructural refinement of al-cu alloy during low melt sheared slope casting. *J. Mater. Eng. Perform.* **2014**, *23*, 439–443. [CrossRef]
42. El Aal, M.I.A.; Kim, H.S. Wear properties of high pressure torsion processed ultrafine grained Al–7% Si alloy. *Mater. Des.* **2014**, *53*, 373–382. [CrossRef]
43. Nie, M.; Wang, C.T.; Qu, M.; Gao, N.; Wharton, J.A.; Langdon, T.G. The corrosion behaviour of commercial purity titanium processed by high-pressure torsion. *J. Mater. Sci.* **2014**, *49*, 2824–2831. [CrossRef]
44. Wang, X.; Nie, M.; Wang, C.T.; Wang, S.C.; Gao, N. Microhardness and corrosion properties of hypoeutectic Al-7Si alloy processed by high-pressure torsion. *Mater. Des.* **2015**, *83*, 193–202. [CrossRef]
45. Gebril, M.A.; Omar, M.Z.; Mohamed, I.F.; Othman, N.K.; Irfan, O.M. Combining Heat Treatment and High-Pressure Torsion to Enhance the Hardness and Corrosion Resistance of A356 Alloy. *Metals* **2022**, *12*, 853. [CrossRef]
46. Cepeda-Jiménez, C.M.; Orozco-Caballero, A.; García-Infanta, J.M.; Zhilyaev, A.P.; Ruano, O.A.; Carreño, F. Assessment of homogeneity of the shear-strain pattern in Al–7 wt% Si casting alloy processed by high-pressure torsion. *Mater. Sci. Eng. A* **2014**, *597*, 102–110. [CrossRef]
47. Descartes, S.; Desrayaud, C.; Rauch, E.F. Inhomogeneous microstructural evolution of pure iron during high-pressure torsion. *Mater. Sci. Eng. A* **2011**, *528*, 3666–3675. [CrossRef]
48. Edalati, K.; Fujioka, T.; Horita, Z. Microstructure and mechanical properties of pure Cu processed by high-pressure torsion. *Mater. Sci. Eng. A* **2008**, *497*, 168–173. [CrossRef]
49. Kawasaki, M. Different models of hardness evolution in ultrafine-grained materials processed by high-pressure torsion. *J. Mater. Sci.* **2014**, *49*, 18–34. [CrossRef]
50. Almazrouee, A.I.; Al-Fadhalah, K.J.; Alhajeri, S.N.; Langdon, T.G. Microstructure and microhardness of OFHC copper processed by high-pressure torsion. *Mater. Sci. Eng. A* **2015**, *641*, 21–28. [CrossRef]
51. Mohamed, I.F.; Masuda, T.; Lee, S.; Edalati, K.; Horita, Z.; Hirosawa, S.; Matsuda, K.; Terada, D.; Omar, M.Z. Strengthening of A2024 alloy by high-pressure torsion and subsequent aging. *Mater. Sci. Eng. A* **2017**, *704*, 112–118. [CrossRef]
52. Cepeda-Jiménez, C.M.; García-Infanta, J.M.; Zhilyaev, A.P.; Ruano, O.A.; Carreño, F. Influence of the thermal treatment on the deformation-induced precipitation of a hypoeutectic Al–7 wt% Si casting alloy deformed by high-pressure torsion. *J. Alloys Compd.* **2011**, *509*, 636–643. [CrossRef]
53. Ghosh, K.S.; Gao, N.; Starink, M.J. Characterisation of high pressure torsion processed 7150 Al–Zn–Mg–Cu alloy. *Mater. Sci. Eng. A* **2012**, *552*, 164–171. [CrossRef]
54. Loucif, A.; Figueiredo, R.B.; Baudin, T.; Brisset, F.; Langdon, T.G. Microstructural evolution in an Al-6061 alloy processed by high-pressure torsion. *Mater. Sci. Eng. A* **2010**, *527*, 4864–4869. [CrossRef]
55. Gebril, M.A.; Omar, M.Z.; Mohamed, I.F.; Othman, N.K.; Irfan, O.M. Microstructure Refinement by a Combination of Heat Treatment and Thixoforming Process Followed by Severe Plastic Deformation and Their Effects on Al-Si Alloy Hardness. *Metals* **2022**, *12*, 1972. [CrossRef]

Disclaimer/Publisher's Note: The statements, opinions and data contained in all publications are solely those of the individual author(s) and contributor(s) and not of MDPI and/or the editor(s). MDPI and/or the editor(s) disclaim responsibility for any injury to people or property resulting from any ideas, methods, instructions or products referred to in the content.